https://dx.doi.org/10.1016/j.combustflame.2024.113371

Experimental and modeling study of NO_2 addition effects on autoignition behavior of propylene

Fuquan Deng[a,b], Xinbo Huang[a], Song Cheng[b], Yingjia Zhang[c], Zuohua Huang[c], Hui Tang[b], Hongtao Zheng[a] , Liu Xiao[a*]

a. College of Power and Energy Engineering, Harbin Engineering University, Harbin, 150001, People's Republic of China.

b. Department of Mechanical Engineering, The Hong Kong Polytechnic University, Kowloon, Hong Kong SAR, People's Republic of China.

c. State Key Laboratory of Multiphase Flows in Power Engineering, Xi'an Jiaotong University, Xi'an 710049, People's Republic of China

***Corresponding author:**

Xiao Liu

Telephone: 86 – 15546378072.

E – mail: liuxiao_heu@163.com (Xiao Liu)

Abstract: Autoignition behaviors of $NO_2/C_3H_6/O_2/Ar$ mixtures with the blending ratio of $[NO_2]/[C_3H_6]$ ranging from 0% to 100% were measured at pressure of 2.03E+5 - 1.01E+6 Pa, temperature of 950 – 1820 K, and equivalence ratio of 0.5 – 2.0 in a high-pressure shock tube. NO_2 blending effects are characterized through changes in ignition delay times. Experiments indicate the strong promoting effect of NO_2 on the reactivity of propane, with greater impacts observed at elevated pressures, lower temperatures, and fuel-leaner conditions. A chemical kinetic model is also proposed, with incorporating the unique and direct interactions between NO_x and propylene and its primary derivatives. Comparison against available experiments and across different models highlight the commendable performance of the updated model, where the updated model out-performs the existing models, both quantitatively and qualitatively, in replicating the propylene autoignition behaviors and oxidation species profiles. Sensitivity and flux analyses are further conducted with the updated model, which reveals the unique NO_x interacting chemistry that leads to the diverse NO_2 blending effects. Particularly, NO_2 addition leads to a clear shift in the consumption of C_3H_6 and its primary derivatives (e.g., C_3H_5-A (CH_2=CH-$\dot{C}H_2$), C_3H_5-T (CH_2=$\dot{C}$-CH_3) and IC_3H_7 (CH_3-$\dot{C}$H-CH_3)) toward the direct interacting channels $R+NO_2=RO+NO$, which considerably promotes the system's reactivity. This paper highlights the importance of the unique interactions between NO_x and unsaturated hydrocarbons, which need to be sufficiently represented in chemistry models in order to accurately predict the complicated effects of EGR.

Keywords*:* NO_2; Propylene; Shock Tube; Ignition Delay Time; Kinetic Analysis

Novelty and Significance Statement

- Autoignition behavior is experimentally characterized for the first time for NO_2 and C_3H_6 mixtures in the intermediate to high temperature regimes. The dataset is particularly valuable toward understanding the NO_2 blending effects on the autoignition of unsaturated hydrocarbons.
- An updated model for propylene/NO_x mixtures is proposed, which incorporates the unique and direct interactions between NO_x species and propylene and its primary derivatives.
- The model is validated comprehensively against the available experimental data from this study and literature, with much better agreements observed in comparison to other models.
- The important interaction kinetics governing the diverse NO_2 blending effects on unsaturated hydrocarbons autoignition are revealed.

Authors Contributions statement

Fuquan Deng: Original draft preparation, Model development, Kinetic analysis, Review & editing, Funding acquisition. **Xinbo Huang**: Data analysis, Validation. **Song Cheng:** Conceptualization, Original draft preparation, Review & editing. **Yingjia Zhang**: Experimental measurement, Review & editing. **Zuohua Huang**: Methodology, Resources, Review & editing. **Hui Tang:** Resources, Review & editing, Supervision. **Hongtao Zheng:** Designed research, Review & editing. **Xiao Liu**: Conceptualization, Resources, Review & editing, Funding acquisition, Supervision.

1 Introduction

Exhaust Gas Recirculation (EGR) is a sophisticated technology for mitigating NO_x emissions in internal combustion engines and is extensively applied in the emerging low-temperature combustion strategies[1, 2]. EGR recirculates a portion of exhaust gases back into the combustion chamber to lower its temperature. Nevertheless, nitrogen oxides (NO_x) in the exhaust gases are also recirculated back into the combustion chamber through EGR, where they undergo intense interactions with hydrocarbons. Recent research has found that even a small amount of nitrogen oxides (NO_x) may have a significant impact on the ignition characteristics and combustion process of fuel, potentially inducing engine knocking. Foucher et al.[3, 4] and Zheng et al.[5] studied the effect of NO/NO_2 on the combustion of n-heptane, isooctane, and toluene under various initial conditions in a HCCI engine. Their findings revealed that 10-100 ppm of NO/NO_2 can significantly promote the ignition process of fuel at low and high temperatures, potentially resulting in engine knocking. Kawabata et al.[6] also confirmed that an increase in NO_x concentration of the residual gas enhances the likelihood and intensity of knocking. Therefore, the influence of NO_x on the combustion characteristics of hydrocarbon fuels is crucial for the design and precise regulation of engines equipped with EGR system.

The interaction between NO_x and hydrocarbon is significantly affected by both fuel molecular structure and the operational conditions. Gasoline and diesel components exhibit intricate structural features, including straight-chain alkanes, branched-chain alkanes, olefins, aromatic hydrocarbons, and various other constituents[7], which poses a notable challenge in developing a detailed chemical reaction kinetic mechanism for NO_x/hydrocarbons chemistry. In recent decades, extensive research has been carried out [8-13] to explore the interaction between NO_x and saturated alkanes. These investigations have illuminated that NO_x has a profound promoting effect on the ignition delay and flame propagation velocity of saturated alkanes, while also significantly altering their species concentration profiles. The promoting effect of NO_x

92 is particularly dependent on various factors, including carbon chain length, temperature,
93 pressure, and equivalence ratio. Specially, Cheng et al.[14, 15] undertook experimental
94 and kinetic investigations to elucidate the influence of nitric oxide (NO) on the low-
95 temperature ignition and heat release characteristics of a gasoline surrogate. Their
96 findings indicate a non-linear promoting effect of NO on the overall reactivity of the
97 gasoline surrogate over low-to-intermediate temperature range, which highlights the
98 critical importance of interactions between hydrocarbons and NO_x in precisely
99 predicting the intricate repercussions linked to exhaust gas recirculation (EGR).
100 However, only a limited number of investigations were conducted on the interaction
101 between NO_x and unsaturated alkenes. Specifically, Menon et al.[16] examined the
102 influence of NO_x (NO, NO_2, and N_2O) on the concentration of soot precursors and soot
103 emission during the pyrolysis of ethylene in a flow reactor. The experimental results
104 revealed significant effects of NO_x on the oxidation rate of ethylene, soot emission, and
105 the concentration of soot precursors. Glarborg et al.[17] investigated concentration
106 profiles of NO/C_2H_4 mixtures in a flow reactor. Their experimental results indicated
107 that NO reduces the initiation temperature threshold for ethylene oxidation by
108 approximately 80-100 K. Deng et al.[18] explored the high-temperature chemical
109 reaction kinetics involving NO_2/C_2H_4 in a high-pressure shock tube. The findings
110 illustrate a significant decrease in the ignition delay time of ethylene at the presence of
111 NO_2. Recently, Yuan et al.[19] conducted an experimental investigation to elucidate the
112 interaction between propylene and NO_x over a temperature range of 725-1250 K using
113 a laminar flow reactor. They found that the promoting effect of NO_x on the oxidation
114 of propylene originates from the reactions between allyl radicals and NO_2 at low
115 temperature.
116 Propylene is a crucial intermediate in the combustion of larger hydrocarbons, and the
117 kinetics model for NO_x/C_3H_6 serves as the core mechanisms in NO_x/larger-
118 hydrocarbons chemistry. However, currently no work has been reported in literature
119 regarding the auto-ignition and kinetic analysis of C_3H_6/NO_2 mixtures under high

120 temperature and elevated pressure. To bridge this gap, the primary objective of this
121 study is to investigate the promoting effect of NO_2 on high temperature autoignition of
122 C_3H_6 using a shock tube. Subsequently, a detailed chemical kinetics mechanism ***is***
123 formulated to accurately describe the ignition chemistry for NO_x/C_3H_6 mixtures, which
124 ***is*** employed to uncover the underlying promoting-mechanisms of NO_2 on C_3H_6 ignition.

125 **2 Experimental**

126 Experiments were conducted in a stainless steel shock tube, which was described well
127 in our previous works[20, 21]. Briefly, a shock tube with an 0.115m internal diameter
128 is divided by a double diaphragm machine into a 4.0-m long driver-section and a 4.8-
129 m long driven-section. The test mixtures were prepared in a 128-L stainless steel mixing
130 tank using the Dalton's law of partial pressure. The partial pressure of each component
131 in the preparing mixtures was monitored by a pressure transmitter (ROSEMOUNT
132 3051). Both the shock tube and mixing tank were evacuated separately to below 1Pa by
133 two mechanical-roots vacuum pump systems before experiments. The leak rate is less
134 than 1 Pa/min in the current situation. The gases used in the experiments were C_3H_6
135 (99.99%), O_2 (99.99%), Ar (99.99%) and NO_2 (diluted by 20% Ar (99.99%)), detailed
136 compositions of the tested mixtures are listed in Table 1. Two different thicknesses of
137 polyethylene terephthalate diaphragms, namely 0.08 mm and 0.25 mm, were used to
138 achieve the target pressures of 2.03E+5 and 1.01E+6 Pa, respectively. He (99.999%)
139 and N_2 (99.999%) were used as the driver gases. As reported by Würmel et al.[22], the
140 valid test time of a shock tube is typically less than 1 ms, the tailored interface method,
141 however, can be used to extend it to several milliseconds. According to the shock theory,
142 the shock tube runs at tailored interactions conditions if meeting the following
143 conditions:

$$\frac{a_3}{a_2}=\frac{\gamma_4\sqrt{1+\frac{\gamma_4+1}{2\gamma_4}\left(p_{52}-1\right)}}{\gamma_1\sqrt{1+\frac{\gamma_1+1}{2\gamma_1}\left(p_{52}-1\right)}} \tag{1}$$

$$\frac{a_4}{a_1}=\frac{2}{\gamma_1+1}\left(M_s-\frac{1}{M_s}\right)\left\{\left[\frac{(\gamma_1-1)M_s^2+2}{2\gamma_1\left(M_s^2-1\right)}\right]\left[\gamma_4^2+\frac{\gamma_1\gamma_4\left(\gamma_4+1\right)\left(M_s^2-1\right)}{(\gamma_1-1)M_s^2+2}\right]^{0.5}+\frac{\gamma_4-1}{2}\right\} \quad (2)$$

$$\frac{a_4}{a_1}=\frac{\sqrt{\gamma_4 W_1 T_4}}{\sqrt{\gamma_1 W_4 T_1}} \quad (3)$$

$$\frac{p_4}{p_1}=\left[1+\frac{2\gamma_1}{\gamma_1-1}\left(M_s^2-1\right)\right]\left[1-\frac{\gamma_4-1}{\gamma_1+1}\frac{a_1}{a_4}\left(M_s-\frac{1}{M_s}\right)\right]^{-\frac{2\gamma_4}{\gamma_4-1}} \quad (4)$$

$$\frac{p_5}{p_1}=\frac{\left[2\gamma_1 M_s^2-\left(\gamma_1-1\right)\right]\left[(3\gamma_1-1)M_s^2-2\left(\gamma_1-1\right)\right]}{\left(\gamma_1+1\right)\left[\left(\gamma_1-1\right)M_s^2+2\right]} \quad (5)$$

$$\frac{T_5}{T_1}=\frac{\left[2\left(\gamma_1-1\right)M_s^2-\left(\gamma_1-3\right)\right]\left[(3\gamma_1-1)M_s^2-2\left(\gamma_1-1\right)\right]}{\left(\gamma_1+1\right)^2 M_s^2} \quad (6)$$

where a_1, a_2, a_3 and a_4 are the local sound velocities in the zone 1, 2, 3 and 4, respectively. $\gamma_1$and γ_4 are the adiabatic index of the mixtures in zone 1 and 4, respectively. M_s is the Mach number of the incident shock. p_{52} is the pressure ratio of p_5 to p_2. W_1 and W_2 are the mean molecular mass in zone 1 and 4, respectively. The typical x-t diagram of a shock tube is given in Figure 1. The parameters in zone 1 (i.e., γ_1, a_1 and T_1) are usually known, and T_4 is usually the ambient temperature. For a given p_5 and T_5, M_s can be calculated by equation (6), and p_1 is obtained from equation (5). p_4 can be determined if the parameters in zone 4 (γ_4 and a_4) are known. So, we can realize tailored conditions in a shock tube by changing the gas state parameters (γ_4 and W_4) of zone 4. Three time-interval counters (FLUKE PM6690) triggered by four pressure transducers (PCB 113B26) with the same distance (0.3m) located in the last 1.3-m long test section of the shock tube with the same interval of 0.3m, were used to obtain the incident shock wave velocities at the end-wall according to the assumption of linear shock attenuation. Chemical equilibrium program Geseq[23] was applied to determine the reflected shock. While the reflected shock pressure was directly monitored by a pressure transducer (PCB 113B03) installed at the end-wall. A photomultiplier (HAMAMASSU CR131) with a 307 nm narrow filter placed at the end-wall was used to record the OH^* light emission. The ignition delay time in this study is defined as the time interval between

the arrival of reflected shock wave at the end-wall (characterized by a jump in the recorded pressure profiles at the end-wall) and the occurrence of main ignition (corresponding to the intersection of the steepest slope of OH^* emission and the base line), as shown in Figure 2. A pressure rise induced by non-ideal boundary layer (dp/dt = 4%/ms) was observed before the main ignition event in current experiments and it has been considered in our simulations. As stated in our previous work[20], the greatest uncertainty in ignition delay time was estimated at 20% based on contribution from the uncertainty in reflected shock temperature (within 20 K) determined by standard root-mean-squares method. All the simulations in *this work* were performed by CHEMKIN program with SENKIN code[24, 25]. We considered pressure rise rate (dp/dt = 4.0%/ms) in all the calculations by SENKIN/VTIM approach proposed by Chaos et al.[26]. The calculated ignition delay time (τ_{ing}) is defined as the time of the maximum dT/dt which has been demonstrated to reasonably meet the experimental definition.

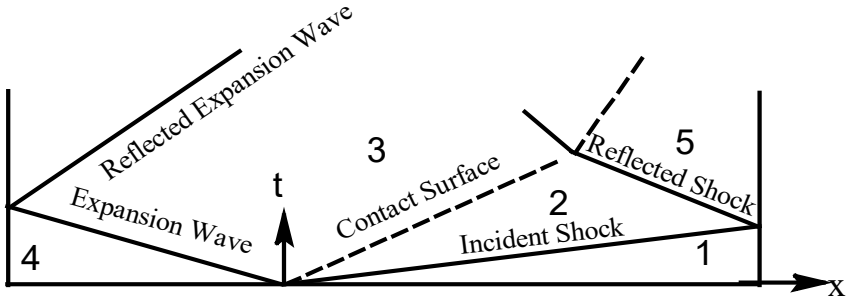

Figure 1 Typical x-t diagram of a shock tube

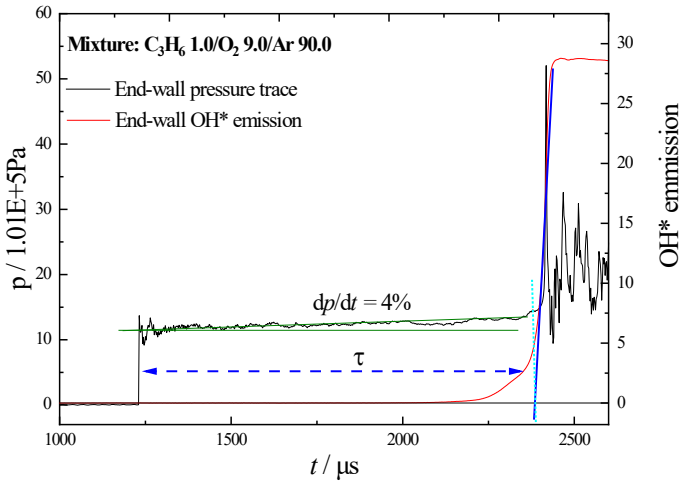

Figure 2 Typical end-wall pressure and OH^* emission profiles for $N_{0/0.5}$ at 1.01E+6 Pa and 1224K.

Table 1. The detail constitutes of four mixtures studied in current experiment.

No.	Mix	Mole blending ratio	C_3H_6 (%)	NO_2 (%)	O_2 (%)	Ar (%)	Φ
1	$N_{0/1.0}$	0% NO_2/100% C_3H_6	1	0	4.5	94.5	1.0
2	$N_{30/1.0}$	30%NO_2/100% C_3H_6	1	0.3	4.5	94.2	1.0
3	$N_{100/1.0}$	100%NO_2/100% C_3H_6	1	1	4.5	93.50	1.0
4	$N_{0/0.5}$	0%NO_2/100% C_3H_6	1	0	9	90	0.5
5	$N_{30/0.5}$	30%NO_2/100% C_3H_6	1	0.3	9	89.7	0.5
6	$N_{0/2.0}$	0%NO_2/100% C_3H_6	1	0	2.25	96.75	2.0
7	$N_{30/2.0}$	30%NO_2/100% C_3H_6	1	0.3	2.25	96.45	2.0

3 Chemical kinetic model

In this study, the Mohamed model[27] and Yuan model[19], both of which account for the C_3/NO_x interaction chemistry, were selected as the tested targets to evaluate their predictive performances against the measured ignition data. Figure 3 presents the comparisons between the experimental observations and predictions of the two selected models for pure C_3H_6/O_2/Ar mixtures at p = 2.03E+5 – 1.01E+6 Pa and φ = 0.5 – 2.0. The results indicate that the Mohamed model[27] reproduces the ignition delay times and reactivity of pure C_3H_6 well over the entire tested range. In contrast, the Yuan model only exhibits satisfactory agreement with the ignition delay times for $N_{0/2.0}$ at p = 2.03E+5 Pa, while over-predicting IDTs for the remaining measured conditions, with the deviation increases with increasing pressure and decreasing equivalence ratio. Specifically, at p = 1.01E+6 Pa and T = ~1300 K, the Yuan model overestimates the ignition delay times of $N_{0/0.5}$, $N_{0/1.0}$ and $N_{0/2.0}$ by around 98.9%, 61.3% and 46.7%, respectively.

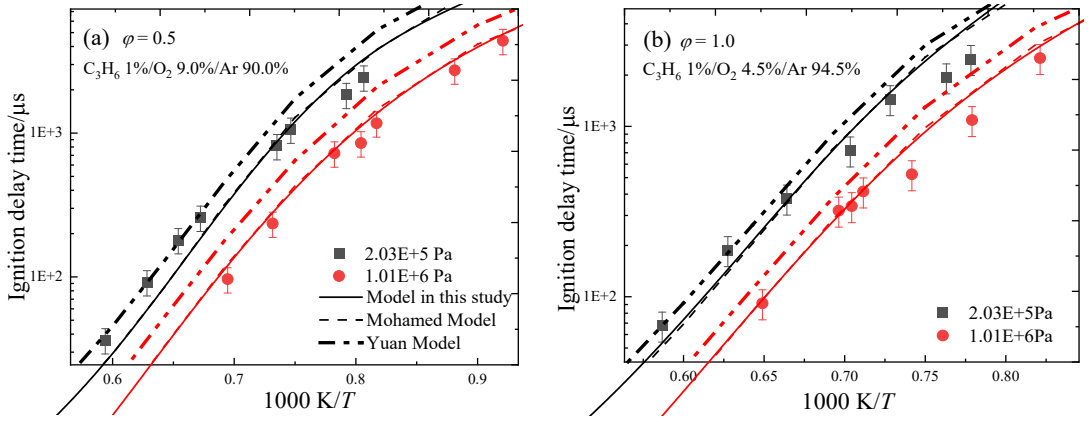

(a) φ = 0.5 (b) φ = 1.0

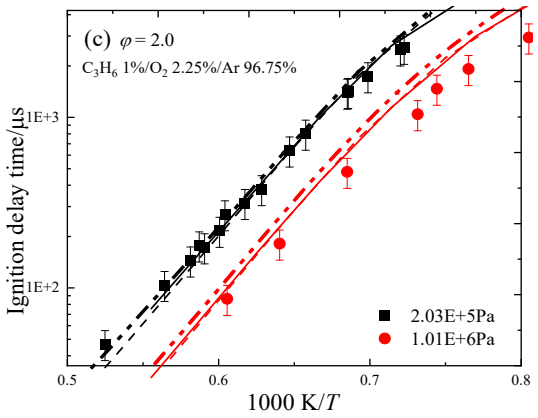

(c) φ = 2.0

194 Figure 3 Comparison between the measured ignition delay times and the model predictions for
195 C_3H_6/O_2/Ar mixtures at φ = 0.5-2.0 and p = 2.03E+5 – 1.01E+6 Pa.

196 Figure 4 illustrates the simulations of both the Mohamed model and the Yuan model for
197 C_3H_6/NO_2 mixtures at p = 2.03E+5 – 1.01E+6 Pa and φ = 0.5 – 2.0. The results indicate
198 that the Mohamed model accurately predicts the ignition delay times for $N_{30/2.0}$ and
199 $N_{30/1.0}$ at the entire pressure range, but severely overestimates the ignition delay times
200 of both $N_{30/0.5}$ and $N_{100/10}$ mixtures, particularly under low temperature and elevated
201 pressure conditions. It can be inferred that the Mohamed model can agree well with the
202 measured data under conditions where NO_2 has little effect on the propylene ignition,
203 while it tends to under-predict the ignition delay times under conditions where great
204 NO_x-promoting effect is observed. This may stem from the lack of specific optimization
205 of the Mohamed model for the C_3H_6/NO_x chemistry. In contrast, the Yuan model could
206 better capture the changing trend of the ignition delay times when varying NO_2
207 concentrations. Specifically, the Yuan model well agrees with the measured data for
208 $N_{30/2.0}$ and $N_{30/1.0}$ within the entire pressure range, as shown in Figure 4 (b) and (d).
209 Moreover, it showcases good agreement with the ignition delay times for $N_{30/0.5}$ at
210 2.03E+5 Pa and $N_{100/1.0}$ at 1.01E+6 Pa. However, it under-predicts by approximately
211 100% and 81% for $N_{30/0}$ at $T \approx$ 1100 K and p = 1.01E+6 Pa (see in Figure 4 (a)), and
212 for $N_{100/1.0}$ at $T \approx$ 1100 K and p = 2.03E+5 Pa (see in Figure 4(c)), respectively. It can
213 be concluded that both the Mohamed model and the Yuan model are unable to
214 adequately capture the ignition delay times of pure C_3H_6 and C_3H_6/NO_x mixtures over

the entire tested conditions.

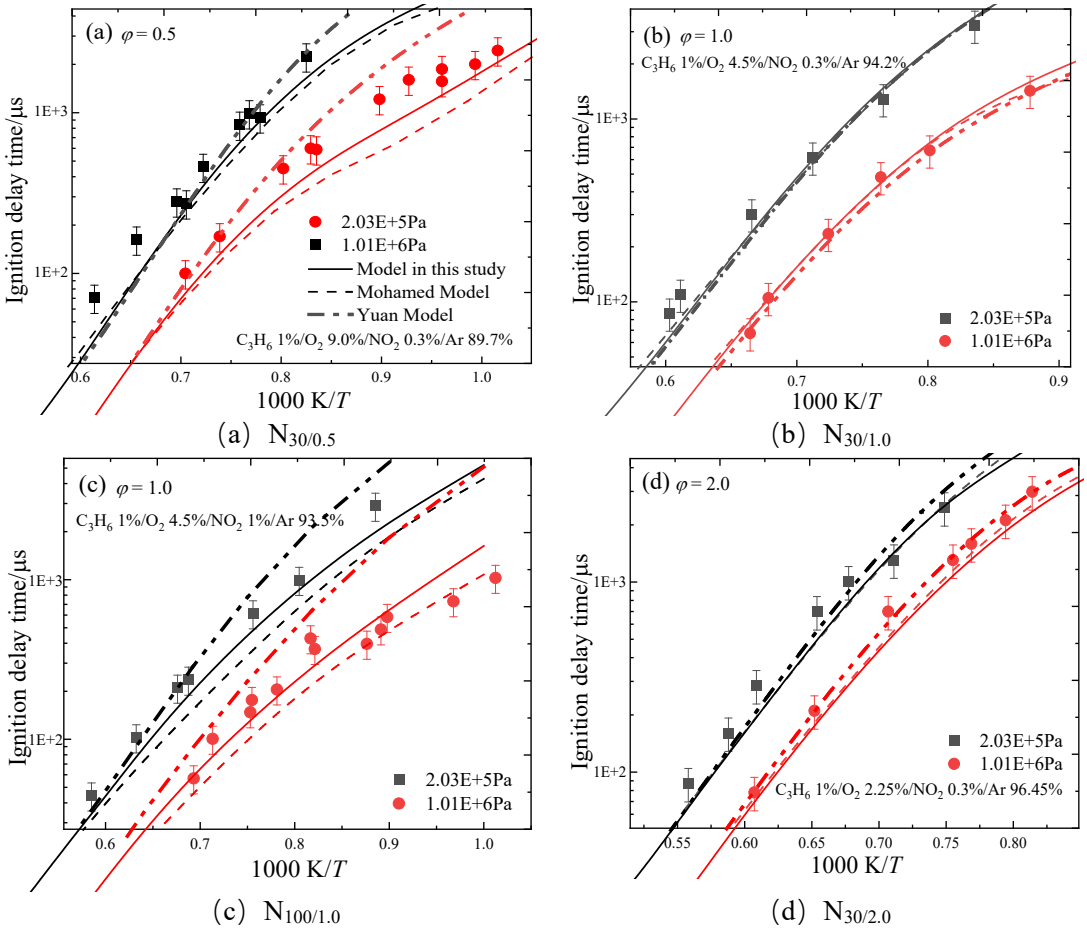

Figure 4 Comparison between the measured ignition delay times and the model predictions for $C_3H_6/NO_2/O_2/Ar$ mixtures at φ = 0.5-2.0 and p = 2.03E+5 – 1.01E+6 Pa.

Therefore, A new model was proposed in this study to validate against the new measured ignition delay times of C_3H_6/NO_x mixtures. The model proposed by Mohamed et al.[27] is selected as the base model, as it has already been extensively validated against a diverse set of the ignition delay times and species profiles of C_3H_6, $CO/H_2/NO_x$ and C_1-C_3 hydrocarbons/NO_x. To describe the direct interactions between NO_2 and propylene, a subset of reactions crucial to the high-temperature combustion chemistry of C_3H_6/NO_2 mixtures was introduced, along with the updated rate parameters. The H-abstraction reactions of $C_3H_6 + NO_2 <=> \dot{C}_3H_5\text{-A} + HNO_2/HONO$ were taken from Chai et al.[28], and the H-abstraction reactions of $C_3H_6 + NO_2 <=> \dot{C}_3H_5\text{-T}/\dot{C}_3H_5\text{-S} + HNO_2/HONO$ were analogous to reactions involving $C_2H_4 + NO_2$[18]. Additionally, $\dot{C}_3H_5\text{-A} + NO_2 <=> C_3H_5O + NO$ were analogous to

$CH_2CH_2OH+NO_2$, whose rate constant was reported by Rissanen et al.[29], and $\dot{C}_3H_5$-T/$\dot{C}_3H_5$-S + NO_2 <=> CH_3COCH_2/CH_3CHCHO + NO were analogous to C_2H_3 + NO_2. Moreover, $C_3H_5NO_2$ <=> $\dot{C}_3H_5$ + NO_2 (including C_3H_5-A, C_3H_5-T and C_3H_5-S) were analogy to reactions concerning NC_3H_7 + NO_2. The $\dot{C}_3H_5$ + NO utilizes the rate constants calculated by Rissanen[29]. All the reactions involving RO_2 + NO (such as CH_2CHCH_2OO, TC_3H_5OO, SC_3H_5OO and AC_3H_5OO, $O_2C_2H_4OH$, $CH_3CH(OO)CHO$, O_2CH_2CHO, $TQJC_3H_6OH$ and $IQJC_3H_6OH$) were referenced to CH_3O_2 + NO. The reactions C_3H_4-A/C_3H_4-P + NO_2 <=> HONO + C_3H_3 were extracted from Wu et al.[30]. C_2H_5CHO/C_2H_3CHO + NO_2 <=> C_2H_5CO/C_2H_3CO + HONO/HNO_2 were analogous to CH_3CHO + NO_2. And the reactions of C_2H_5CO/C_2H_3CO + NO_2 <=> C_2H_5/C_2H_3 + CO_2 + NO were analogous to CH_3CO + NO_2. All the important improvement based on the Mohamed model has been listed in Appendix, and the whole updated C_3H_6/NO_x mechanism is provided in ***Supplementary material***.

As shown in Figure 3 and Figure 4, in contrast to the Mohamed model and the Yuan model, the model updated in this study quite well reproduces the ignition delay times and reactivity of C_3H_6 mixtures with and without NO_2 at the entire tested conditions. As shown in the ***Supplementary material***, the new model has also been validated against the species profiles for $C_3H_6/NO/NO_2$ mixtures measured in a flow reactor at various equivalence ratios by Yuan et al.[19], and against the species profiles for C_3H_6/NO mixtures obtained from a jet-stirred reactor according to Dagaut et al.[31], then against the evolutions of C_3H_6 and NO_2/NO_x ratio with residence time for C_3H_6/NO/air mixtures over temperatures ranging from 600 K to 1200 K in the presence of 20 ppm NO measured by Hori et al.[32], as well as against the ignition delay time of C_3H_6/NO mixtures measured in flow reactor by Gokulakrishnan et al.[33]. Consequently, the ignition delay times and species profiles collected in the related literatures are also overall quite well reproduced by the model developed in this study. Therefore, the proposed model is used to analyze the ignition behaviors and kinetic analyses for C_3H_6/NO_x mixtures in next sections.

4 Results and discussion

Figure 5 illustrates the effect of NO_2 on the C_3H_6 ignition at p = 2.03E+5 – 1.01E+6 Pa and φ = 0.5 with 30% NO_2 addition. It can be seen that the presence of NO_2 exerts a minimal effect on the propylene ignition at p = 2.03E+5 Pa over the measured temperature range. Additionally, under elevated pressure conditions (1.01E+6 Pa), the introduction of 30% NO_2 likewise presents a modest impact on the ignition delay times when T > ~1160 K. However, when T falls below 1160 K, the NO_2 addition significantly decreases the ignition delay time of the combustion mixtures. In more detail, at p = 1.01E+6 Pa, 30% NO_2 addition gives a reduction about 79% and 46% in the ignition delay time at $T \approx$ 1080 K and 1250 K, respectively.

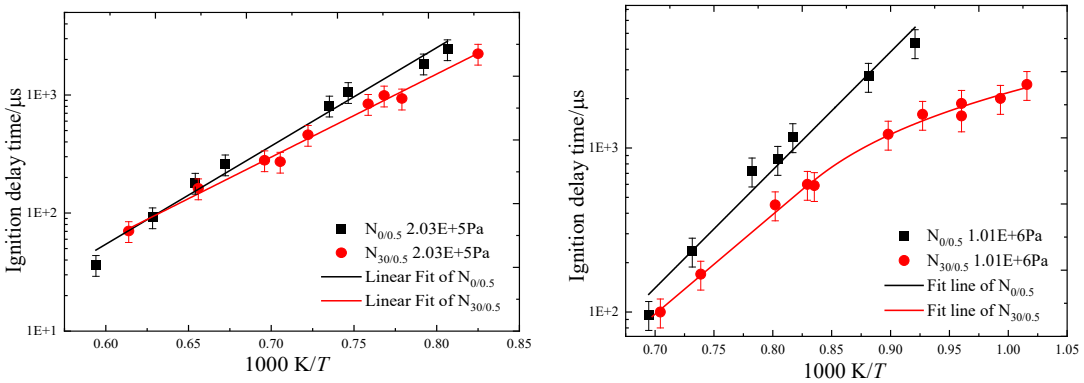

(a) 2.03E+5 Pa (b) 1.01E+6 Pa

Figure 5 Effects of NO_2 addition on the propylene ignition at φ = 0.5.

Figure 6 shows the impact of NO_2 on the stoichiometric propylene ignition with $[NO_2]/[C_3H_6]$ varying from 30% to 100% at p = 2.03E+5 and 1.01E+6 Pa. The introduction of NO_2 is observed to substantially enhance the reactivity of propylene, and the promoting effect is more pronounced with higher NO_2 concentrations and higher pressure, as well as lower temperature. The presence of 30% NO_2 exerts a negligible effort on propylene ignition at p = 2.03E+5 Pa over the measured temperature range, which is consistent with the similar finding in the case of φ = 0.5. However, with higher NO_2 addition or at elevated pressure, considerable reductions in the ignition delay time are observed. Specifically, at $T \approx$ 1285 K, $N_{30/1.0}$ and $N_{100/1.0}$ respectively reduces the ignition delay time by 39% and 71% at p = 2.03E+5 Pa and by 55% and

79% at p = 1.01E+6 Pa.

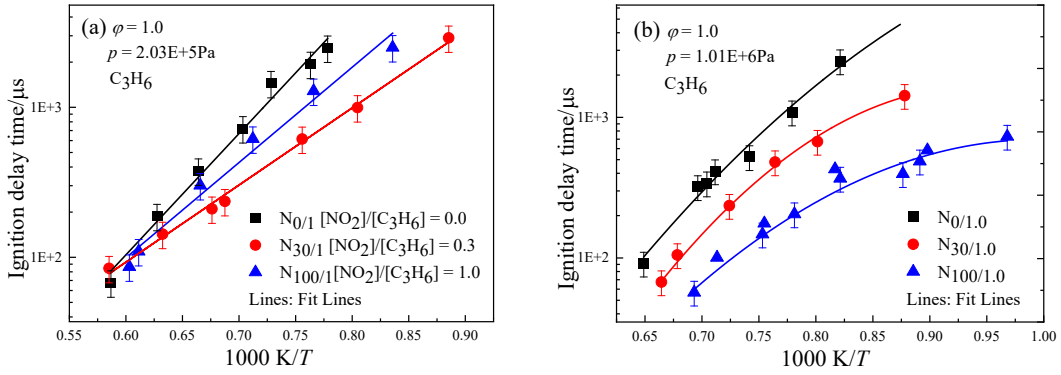

(a) 2.03E+5 Pa (b) 1.01E+6 Pa

Figure 6 Effects of NO_2 addition on the propylene ignition at φ = 1.0.

Figure 7 shows the influence of 30% NO_2 addition on the ignition delay times of fuel-rich (φ=2.0) propylene mixture over a pressure range of 2.03E+5 to 1.01E+6 Pa. The results show that the NO_2 addition barely impacts the propylene ignition at 2.03E+5 Pa for $N_{30/2.0}$. However, at p = 1.01E+6 Pa and T > ~1450 K, no obvious reduction in the ignition delay times is observed with 30% NO_2 addition. NO_2 only exhibits a slight promoting-effect on the ignition of C_3H_6 at p = 1.01E+6 Pa and T < ~1450 K. In summary, the extent of NO_2 promoting-effect on the ignition delay times of C_3H_6 varies with pressure and temperature as well as equivalence ratio, with the most significant impact being observed at elevated pressure, low temperature, and fuel-lean conditions.

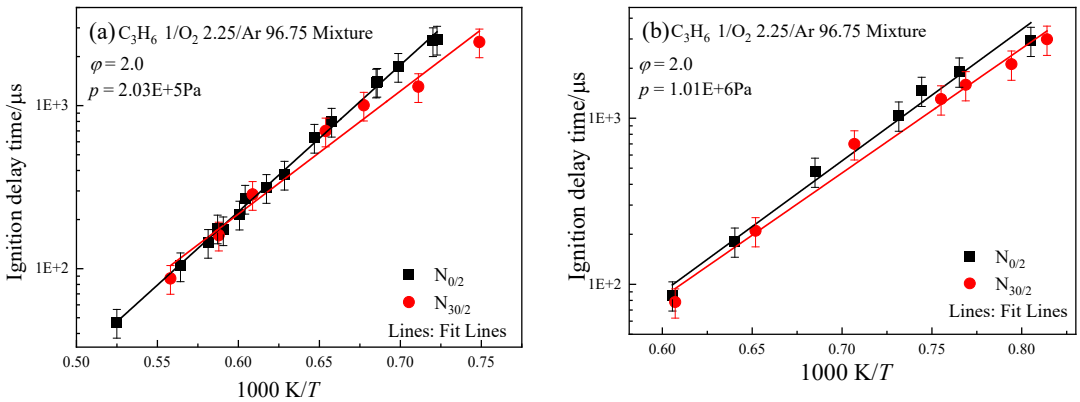

(a) 2.03E+5 Pa (b) 1.01E+6 Pa

Figure 7 Effects of NO_2 addition on the propylene ignition at φ = 2.0.

The impact of equivalence ratio on the autoignition behavior of pure C_3H_6 and C_3H_6/NO_2 mixtures are summarized in Figure 6 and Figure 7, respectively. As shown in Figure 8 and 9, the ignition delay times give a clear Arrhenius dependence on

293 temperature for C_3H_6/O_2/Ar mixtures with and without NO_2 addition over equivalence
294 ratio of 0.5-2.0, except for $N_{30/0.5}$ at p = 1.01E+6 Pa when T < 1100K. As reported by
295 Davidson et al.[34], the ignition delay time exhibits an simple Arrhenius-dependence
296 for a given mixture, as the flowing:

$$\tau = A\varphi^m p^n \, exp(\, E_a/RT) \tag{7}$$

297 where τ is ignition delay time (μs), T is temperature (K), φ is equivalence ratio, p is
298 pressure (Pa) and E_a is the global activation energy (kcal/mol), R is the universal gas
299 constant (kcal·mol^{-1}K^{-1}). The Arrhenius correlations fitted from the experimental data
300 are shown as follows:
301 C_3H_6 mixtures without NO_2:

$$\tau = 3.68 \times 10^{-7} \times \varphi^{1.079} \times p^{-0.639} \times exp(\, 36.91/RT) \tag{8}$$

302 C_3H_6 mixtures doped with 30% NO_2 (except for $N_{30/0.5}$ at p = 1.01E+6 Pa in T < 1100K):

$$\tau = 5.62 \times 10^{-6} \times \varphi^{1.105} \times p^{-0.694} \times exp(\, 30.824/RT) \tag{9}$$

303 $N_{30/0.5}$ (at 1.01E+6 Pa in T < 1100 K):

$$\tau = 18.74 \, exp(\, 9.41/RT) \tag{10}$$

304 It is noted that the presence of NO_2 leads to a noticeable decrease in the global activation
305 energy within the equivalence ratio range of 0.5-2.0. This suggests a substantial
306 enhancement in the system's reactivity due to the presence of NO_2. The global
307 activation energies are 36.91 kcal/mol for the pure propylene mixtures (seen in Eq.(8))
308 and 30.82 kcal/mol for propylene mixtures doped with 30% NO_2 (seen in Eq.(9)),
309 except in the case of $N_{30/0.5}$ at p = 1.01E+6 Pa in T <~1100 K. For $N_{30/0.5}$ at 1.01E+6 Pa
310 and T <~1100 K, the global activation energy drastically decreases to 9.41 kcal/mol, as
311 shown in Eq. (10), implying a significant shift in the reactivity-controlling kinetic under
312 high pressure and low temperature conditions. The Arrhenius relationship indicates a
313 positive exponential coefficient for the equivalence ratio, suggesting that the ignition
314 delay time increases with increasing equivalence ratios. Conversely, the exponential
315 coefficient of pressure is negative, implying a decrease in the ignition delay time as
316 pressure rises. Notably, the ignition delay times become much more sensitive to the

variations in pressure and equivalence ratio upon the introduction of NO_2 to propylene.

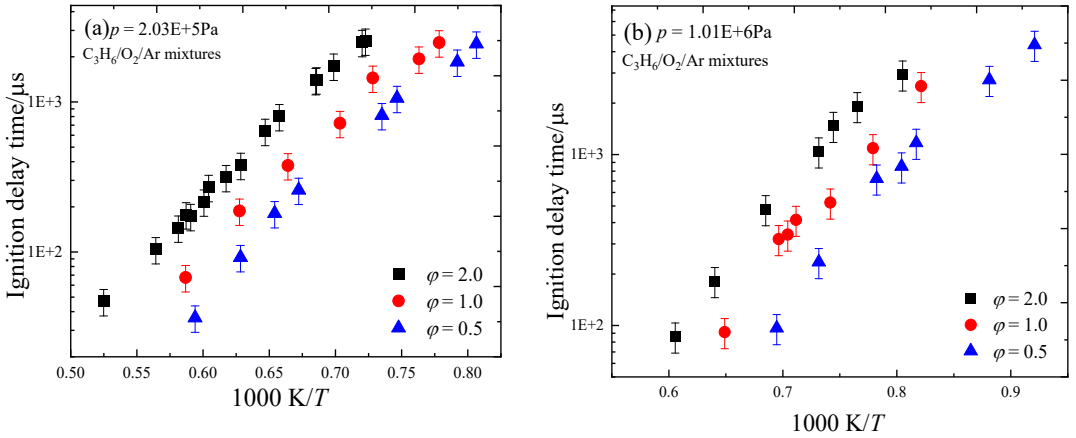

(a) p = 2.03E+5 Pa (b) p = 1.01E+6 Pa

Figure 8 Effect of equivalence ratio on the ignition of pure propylene mixtures.

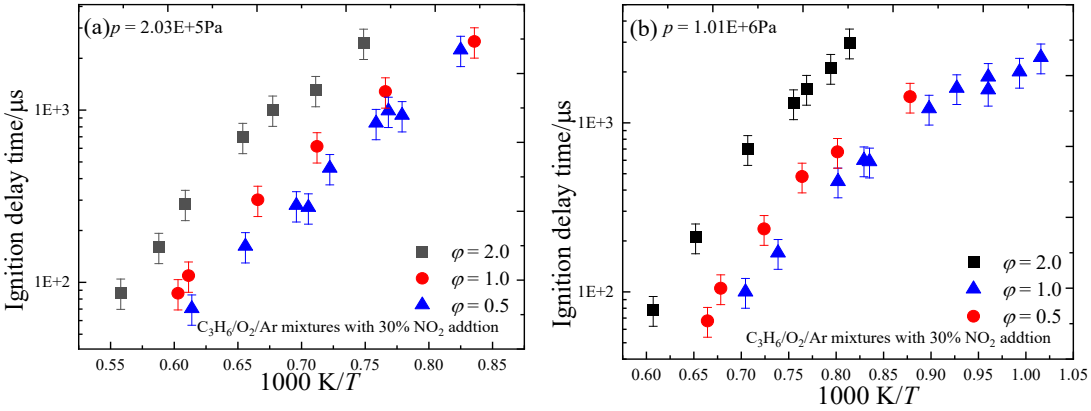

(a) p = 2.03E+5 Pa (b) p = 1.01E+6 Pa

Figure 9 Effect of equivalence ratio on mixtures doped with 30% NO_2.

5 Kinetic analysis

To gain chemical insights into the promoting-effect of NO_2 on the propylene ignition under different conditions, the model developed in this study was applied for a brute-force sensitivity analysis and a flux analysis for the stoichiometric C_3H_6/NO_2 mixtures at p = 2.03E+5 Pa and T = 1650 K to interpret the weak effect of NO_2, and at p = 1.01E+6 Pa and T = 1000 K to identify the reactivity-controlling chemistry dominating the considerable promoting-effect of NO_2, respectively. The flux analysis was conducted at the reaction time corresponding to 10% consumption of propylene, and the normalized sensitivity coefficient is defined as[35]:

$$S_i = \frac{\tau(2k_i) - \tau(0.5k_i)}{1.5\tau(k_i)} \tag{11}$$

Where τ is the ignition delay time (μ s), k_i and S_i are the rate constant and sensitivity

coefficient of i^{th} reaction, respectively. A negative value means promoting effect on reactivity and vice versa.

5.1 Sensitivity analysis and flux analysis at low pressure and high temperature

Figure 10 illustrates the twenty-five most-sensitive reactions for the stoichiometric $C_3H_6/O_2/Ar$ mixture with and without NO_2 addition at 2.03E+5 Pa and 1650 K to interpret the small promoting-effect of NO_2 on the propylene ignition. In the case of the pure propylene mixture, it is evident that the chain branching reaction R10 ($O_2 + H <=> O + OH$) overwhelmingly controls its ignition process, while the remaining reactions exhibit comparatively lower sensitivity coefficients. This is because that R10 consumes a single H atom and immediately yields two highly reactive O and OH radicals, resulting in an exponential expansion of the radical pool. Besides, it is noteworthy that hydrogen atoms are involved in four-fifths of both the top promoting reactions and the top inhibiting reactions, which highlights the critical role of the generation and consumption of hydrogen atom in C_3H_6 ignition under high-temperature conditions. Specifically, R969 ($C_3H_6 + H <=> CH_3CHOCHO + H$) and R208 ($HCO + H <=> CO + H_2$) emerge as the top two inhibiting reactions, as they compete with R10 for H atoms. In contrast, R998 ($C_3H_6 + O <=> C_3H_5\text{-}A + OH$), R1231 ($C_3H_4\text{-}A + H <=> C_3H_5\text{-}A$) and R959 ($C_3H_6 <=> C_3H_5\text{-}A + H$) feed H atoms to R10, and are thereby ranked as the second, third, and fifth top promoting reactions, respectively. For the stoichiometric $C_3H_6/NO_2/O_2/Ar$ mixtures ($N_{30/1.0}$ and $N_{100/1.0}$), R10 remains the primary governing reaction for the ignition of the $C_3H_6/NO_2/O_2/Ar$ mixtures, whereas the other reactions exert negligible influence. Notably, among the top twenty-five most sensitive reactions for both the $C_3H_6/O_2/Ar$ and $C_3H_6/NO_2/O_2/Ar$ systems, twenty-three reactions are duplicates, and only two less sensitive reactions involve NO_2. The sensitivity analysis indicates minimal alteration in the chemical kinetics dominating the rate-limiting steps underlying the ignition of propylene.

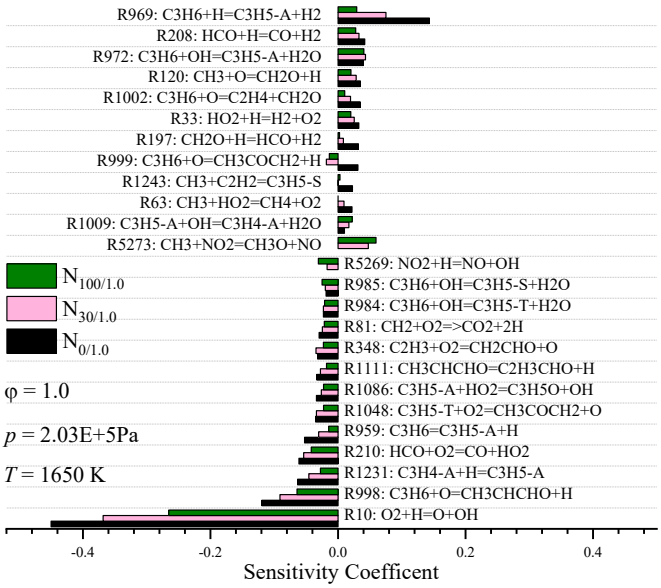

Figure 10 Normalized sensitivity analysis at p = 2.03E+5 Pa and T = 1650 K using the updated model for $C_3H_6/O_2/Ar$ mixtures with and without NO_2 addition.

The main flux analysis for the three measured mixtures at 1650 K and 2.03E+5 Pa is presented in Figure 11. For $N_{0/1.0}$, the consumption of propylene is primarily dominated by the interactions between C_3H_6 and radical pools (including H, O, OH and a small amount of CH_3 radicals). This confirms the predominant influence of R10 during propylene ignition presented in Figure 10. Notably, the branching ratios for H-abstraction reactions *via* C_3H_6 + H/OH/CH_3 to produce the resonance-stabilized allyl radical C_3H_5-A radicals, as well as the C_3H_5-T radicals and C_3H_5-S radicals, constitute approximately 46.8%, 13%, and 7.3%, respectively. Additionally, around 10% of C_3H_6 reacts with O-atoms *via* a chain propagation reaction R998 (C_3H_6 + O <=> CH_3CHCHO + H). Subsequently, the majority of the generated CH_3CHCHO rapidly decomposes *via* a cleavage reaction R1111 (CH_3CHCHO <=> C_2H_3CHO+H). The total process consumed one oxygen atom and generated two reactive hydrogen atoms, promptly feeding the chain branching reaction R10. Consequently, it is not surprising that R998 becomes the second most-promoting reaction. Moreover, approximately 5.1% of C_3H_6 reacts with O-atoms *via* R999 (C_3H_6 + O <=> CH_3COCH_2 + H), and the resulting CH_3COCH_2 then rapidly decomposes into CH_2CO + CH_3. As shown by Dong et al.[36], C_3H_5-A is very vital for the ignition of propylene as it contains the conjugated double

bond, which leads to a significantly lower reactivity of propylene compared to other alkenes. Thus, the primary consumption branching pathways of C_3H_5-A radicals are analyzed in this study. It is noteworthy that the consumption pathway of C_3H_5-A is particularly complex. Up to 47.3% of C_3H_5-A radicals undergo the C–H bond cleavage reaction R1231 (C_3H_4-A+H <=> C_3H_5-A), and the resulting H-atom is fed into R10. Consequently, R1231 emerges as the third most promoting reaction. In addition, approximately 10.1% of C_3H_5-A radicals react with HO_2 via R1086 (C_3H_5-A+HO_2 <=> C_3H_5O+OH), which facilitates the conversion of the less reactive HO_2 radical into the chain-initiating radical OH. Additionally, the produced unstable C_3H_5O is rapidly consumed through the decomposition and isomerization reactions, indicating that this is a fast fuel consumption pathway. As a result, R1086 becomes the seventh most-promoting reaction.

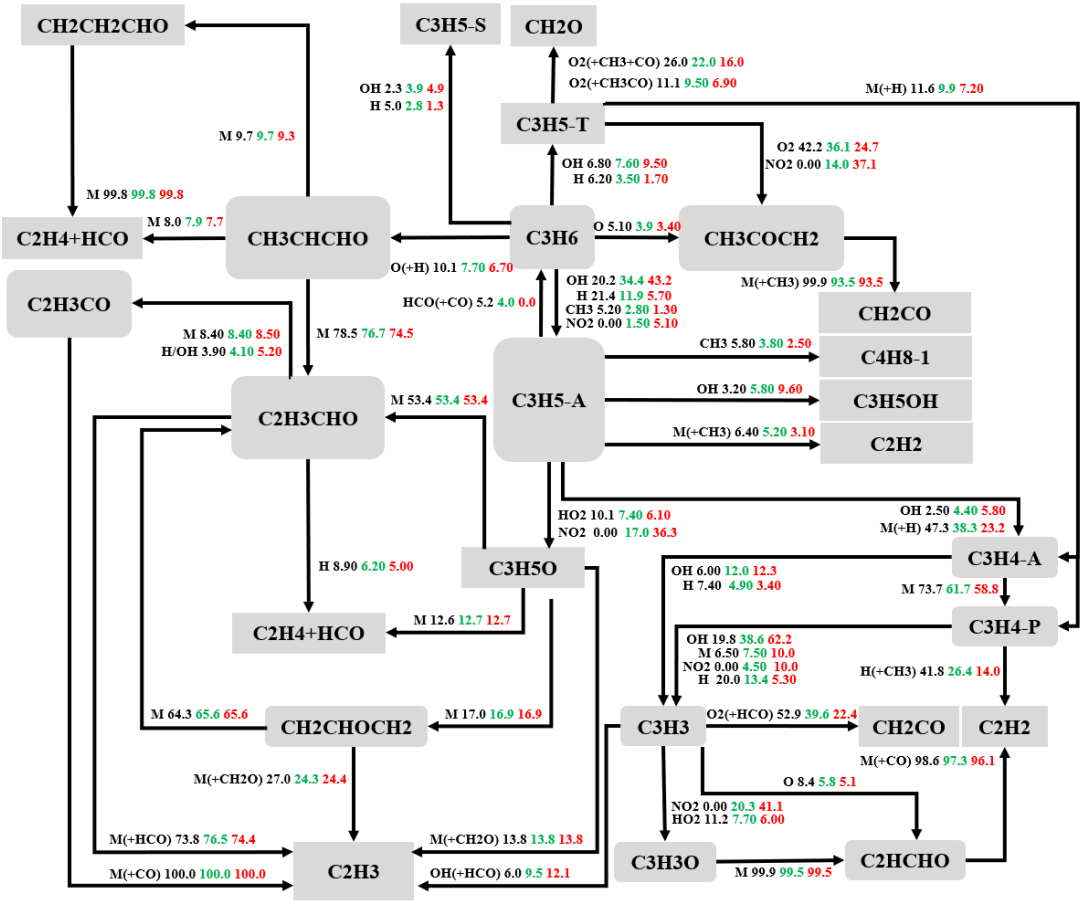

Figure 11 Flux analysis for stoichiometric C_3H_6/NO_2 mixtures at 2.03E+5 Pa, 1650 K and 10% C_3H_6 consumption using the updated model. ($N_{0/1.0}$:Black, $N_{30/1.0}$:Green and $N_{100/1.0}$:Red)

As shown in Figure 11, when NO_2 is introduced into the propylene mixtures, due to the competition between R5269 ($NO_2 + H = NO + OH$) with the chain branching reaction R10 ($O_2 + H <=> O + OH$) to convert H-atom into OH radicals, the branching ratio of C_3H_6 + OH increases significantly, while the branching ratios of C_3H_6 + O/H gradually decrease. However, the presence of NO_2 minimally affects the total branching ratio of C_3H_6 to produce each intermediate (like C_3H_5-A, C_3H_5-T, C_3H_5-S, and others). Besides, the strong oxidizing ability of NO_2 accelerates the fuel consumption rate of propylene radicals (e.g., C_3H_5-A and C_3H_5-T) through the interaction of $R\cdot + NO_2 <=> RO + NO$, thereby enhancing the reactivity of the system. Nevertheless, the production of H atom and/or O atom within the other consumption pathways of propylene radicals is correspondingly reduced, exerting an inhibitory effect on the system's reactivity. Specifically, as the NO_2 blending ratio gradually increases from 0% to 100%, the branching rate for C_3H_5-A consumption *via* R1231 (C_3H_4-A + H <=> C_3H_5-A) gradually decreases from 47.3% to 23.2%, corresponding to a simultaneous increase in R5169 (C_3H_4-A + NO_2 <=> C_3H_5O + NO) from 0% to 36.3%. Similarly, for the case of C_3H_5-T, the branching rate undergoing R1048 (C_3H_5-T + O_2 <=> CH_3COCH_2 + O) gradually reduces from 42.2% to 24.7%, while that *via* R5175 (C_3H_5-T + NO_2 <=> CH_3COCH_2 + NO) increases from 0% to 40.3%. As a result, within the mutually offsetting of promoting kinetics and inhibiting kinetics induced by NO_2, the enhancement of propylene ignition in the presence of NO_2 is comparatively modest.

5.2 Sensitivity analysis and flux analysis at high pressure and low temperature

Figure 12 provides the thirty most sensitive reactions for the stoichiometric $C_3H_6/O_2/Ar$ mixtures, with the NO_2 blending ratio ranging from 0 to 100%, at p = 1.01E+6 Pa and T = 950 K, where the NO_2 addition presents considerable promoting effect on the propylene ignition. Notably, a significant shift in the reactivity-controlling kinetics is observed under the two considered conditions. At high temperature and low pressure, propylene ignition is dominated by chemical kinetics involving the generation and consumption of radical pools, particularly the H-atom. In contrast, at low temperature

and elevated pressure, the propylene ignition is clearly governed by reaction pathways contributing to the consumptions of C_3H_6 and propenyl radicals. For the pure propylene mixture, as depicted in Figure 12，the reactivity-controlling kinetics under lower temperature and elevated pressure conditions display two distinct characteristics. Firstly, both the consumption rate and branching ratios of propylene (C_3H_6) and three propenyl radicals (C_3H_5-A, C_3H_5-S, and C_3H_5-T) play a significant role in determining the system's reactivity. Secondly, there is a notable deficiency of highly reactive free radicals. Apart from HO_2, O_2 and CH_3 radicals yet serve as crucial reactive oxidants to participate in the consumption of propylene and propenyl radicals. Interestingly, CH_3 no longer serves as an intermediate to generate even smaller products. Instead, the majority of CH_3 radicals act as reactive radicals, engaging in either the H-abstraction reaction through R974 (C_3H_6 + CH_3 <=> C_3H_5-A + CH_4) or in addition reactions via R2365 (C_3H_5-A + CH_3(+M) <=> C_4H_8-1(+M)), which clearly suggests a significant scarcity of highly reactive free radicals within the system.

In more details, as depicted in Figure 12, three-fifths of the 30 most sensitive reactions involve C_3H_6 and propenyl radicals. Specifically, the H-abstraction reactions involving C_3H_6 + OH/H can demonstrate dual roles as either promoting or inhibiting reactions. The C_3H_6 + OH reactions *via* R984 (C_3H_6 + OH <=> C_3H_5-T + H_2O) and R985 (C_3H_6 + OH <=> C_3H_5-S + H_2O) rank as the second and fourth most promoting reactions, respectively. This is because the generated C_3H_5-S and C_3H_5-T radicals subsequently react with O_2 to produce allyloxy radicals and O atoms, which can open the double bond in propylene and distinctly enhance the system's reactivity. Conversely, C_3H_6 + OH can also undergo the largest inhibiting reaction, R972 (C_3H_6 + OH <=> C_3H_5-A + H_2O), which changes the reactive OH radical into the stable C_3H_5-A radicals. Similarly, reactions involving C_3H_6 + H either exhibit a inhibitory effect through R1004 (C_3H_6 + H <=> C_2H_4 + CH_3) and R969 (C_3H_6 + H <=> C_3H_5-A + H_2), leading to the transfer of the reactive H atom into stable CH_3 or C_3H_5-A radicals; or demonstrate a promoting effect *via* R1005 (C_3H_6 + H <=> IC_3H_7), where HO_2 radicals can quickly be generated

via R762 (O_2 + IC_3H_7 <=> HO_2 + C_3H_6) to feed the biggest promoting reaction R1086 (C_3H_5-A + HO_2 <=> C_3H_5O + OH). Moreover, R970 (C_3H_6 + O_2 <=> C_3H_5-A + HO_2) becomes the third most significant promoting reaction, as it transforms O_2 into more reactive HO_2 radicals to feed the largest promoting reaction R1086. R973 (C_3H_6 + HO_2 <=> C_3H_5-A + H_2O_2) is another important promoting reaction, as the produced H_2O_2 rapidly decomposes to yield two reactive OH radical. Furthermore, the branching ratio for C_3H_5-A radicals is also crucial in determining the reactivity of propylene. R1086 (C_3H_5-A + HO_2 <=> C_3H_5O + OH) emerges as the largest promoting reaction, as it individually transforms the less-reactive C_3H_5-A and HO_2 radicals into the unstable C_3H_5O and the reactive OH radicals. Conversely, R2365 (C_3H_5-A + CH_3 (+M) <=> C_4H_8-1 (+M)) is ranked as the second most inhibitory reaction due to its competition with R1086 for C_3H_5-A radicals and conversion of C_3H_5-A and CH_3 radicals into a more stable C_4H_8-1.

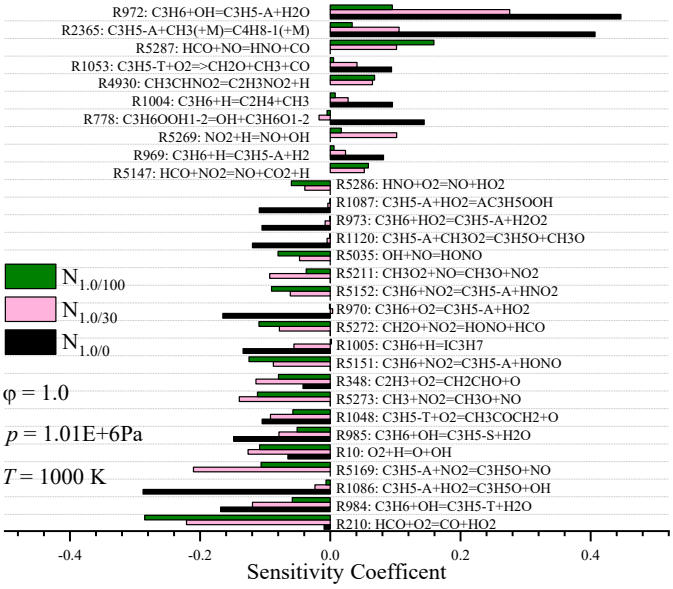

Figure 12 Normalized sensitivity analysis at p = 1.01E+6 Pa and T = 1000 K using the updated model for stoichiometric C_3H_6/O_2/Ar mixtures with and without NO_2.

As depicted in Figure 12, the NO_2 addition induces notable shifts in the 30 most sensitive reactions. This illustrates the substantial role of NO_2 in the reactivity-controlling kinetics dominating the propylene ignition at this performed conditions. Particularly, R210 (HCO + O_2 <=> CO + HO_2) emerges as the biggest promoting

reaction. Subsequently, the produced HO_2 promptly reacts with NO *via* R5045 (NO + $H\dot{O}_2$ <=> NO_2 + $\dot{O}H$), facilitating the generation of chain-initiating OH radicals. As a result, propylene is more preferred to be oxidized by OH radicals, which in turn leads R984 (C_3H_6 + OH <=> C_3H_5-T + H_2O) and R972 (C_3H_6 + OH <=> C_3H_5-A + H_2O) to become a highly sensitive promoting reaction and an extremely sensitive inhibiting reaction, respectively. In contrast, interactions involving C_3H_6 + O_2/HO_2/O, which exhibit pronounced effects in the pure propylene ignition, become negligible. Besides, due to its strong oxidation ability, the NO_2 addition largely drives the consumption of these less-reactive species, resulting in the emergence of many novel and sensitive reaction pathways associated with Fuel + NO_2 interactions. Furthermore, the highly sensitive inhibiting reaction R2365 (C_3H_5-A + CH_3 (+M) <=> C_4H_8-1 (+M)) for the pure propylene becomes insignificant, while R5273 (CH_3 + NO_2 <=> CH_3O + NO) replaces it as the primary promoting reaction in response to NO_2 addition.

To further interpret the significant promoting effect of NO_2 on the propylene ignition under low-temperature and elevated-pressure conditions, the main flux analysis for the three measured mixtures at 1000 K and 1.01E+6 Pa is presented in Figure 13. For $N_{0/1.0}$, the pathways responsible for the consumption of propylene and propenyl radicals are highly intricate, and there is no singular reaction pathway that can dominate the propylene ignition. Particularly, propylene is predominantly consumed through the following four distinct reaction pathways: 1) Approximately 32.7% and 5.9% of C_3H_6 undergo H-abstraction reactions with OH and CH_3 radicals to produce C_3H_5-A. 2) Around 14.5% of C_3H_6 participates in an addition reaction with H atoms to yield IC_3H_7. Subsequently, 80% of the resulting IC_3H_7 rapidly reacts with O_2 *via* R762 (O_2 + IC_3H_7 <=> HO_2 + C_3H_6) to generate HO_2 radicals, which is a primary source of HO_2 radicals in the propylene ignition. 3) Roughly 10.1% of C_3H_6 reacts with HO_2 radicals *via* R777 ($C_3H_6OOH_{1-2}$<=>HO_2+C_3H_6) to produce $C_3H_6OOH_{1-2}$, which promptly decomposes into $C_3H_6O_{1-2}$ + OH. 4) A proportion of 7.6% of C_3H_6 experiences a chain propagation reaction with OH radicals *via* R984 (C_3H_6 + OH <=> C_3H_5-T + H_2O) to form C_3H_5-T

radicals. Additionally, there are six reaction pathways of comparable importance for C_3H_5-A. The branching ratio between C_3H_5-A and HO_2 is either 30.6% leading to the production of the unstable C_3H_5O, or 11.9% resulting in the formation of AC_3H_5OOH, which subsequently decomposes into C_3H_5O + OH. Additionally, up to 23.1% of C_3H_5-A reacts with CH_3 radicals *via* R2365 (C_3H_5-A + CH_3 (+M) <=> C_4H_8-1 (+M)) to produce C_4H_8-1. Furthermore, approximately 12.5% of C_3H_5-A reacts with O_2 to yield CH_3CO + CH_2O via R1032 (C_3H_5-A + O_2 <=> CH3CO + CH_2O); while 9.8% of C_3H_5-A undergoes an addition reaction to produce CH_2CHCH_2OO *via* R5304 (CH_2CHCH_2OO <=> C_3H_5-A + O_2).

For mixtures doped with NO_2 ($N_{30/1.0}$ and $N_{100/1.0}$), the consumption of propylene through reactions between C_3H_6 and OH radicals increase significantly due to the abundant formation of OH radicals at the presence of NO_2. The observation indicates that the branching ratio of R972 (C_3H_6 + OH <=> C_3H_5-A + H_2O) increases to 46.1% and 52.7% for $N_{30/1.0}$ and $N_{100/1.0}$, respectively. Additionally, the branching ratio *via* R984 (C_3H_6 + OH <=> C_3H_5-T + H_2O) rises from 7.6% for $N_{0/1.0}$ to 10.7% and 12.3% for $N_{30/1.0}$ and $N_{100/1.0}$, respectively. Correspondingly, the branching ratio *via* R777 ($C_3H_6OOH_{1\text{-}2}$ <=> HO_2 + C_3H_6) nearly diminishes to 0% due to the impact of the R5045 (NO + $H\dot{O}_2$ <=> NO_2 + $\dot{O}H$). Moreover, the branching ratio of R1005 (C_3H_6 + H <=> IC_3H_7) remains nearly unchanged as the NO_2 blending ratio increases from 0 to 30%, while decreases to 6.5% as the NO_2 blending ratio increases from 30% to 100%. As the NO_2 concentration gradually rises, the branching ratio of C_3H_6 + NO_2 <=> C_3H_5-A + $HONO/HNO_2$ increases up to 7.3%. Noteworthy, the presence of conjugated double bonds in C_3H_5-A results in an extremely lower reactivity of propylene in comparison to the other alkenes[37]. When NO_2 is introduced into propylene mixtures, C_3H_5-A is primarily consumed by the R5169 (C_3H_5-A+NO_2<=>C_3H_5O+NO) reaction, resulting in a notable rise in the consumption rate of C_3H_5-A and the accompanied significant enhancement in the system's reactivity due to the strong oxidizing ability of NO_2. Furthermore, NO_2 also largely enhances the consumption rates of other fuel radicals

R· (e.g., C_3H_5-T, IC_3H_7, CH_3, C_2H_3) and less-reactive intermediate species such as aldehydes RCHO (e.g., C_2H_5CHO, C_2H_3CHO, CH_3CHO, CH_2O), which furtherly contributes to the enhancement of the system's overall reactivity.

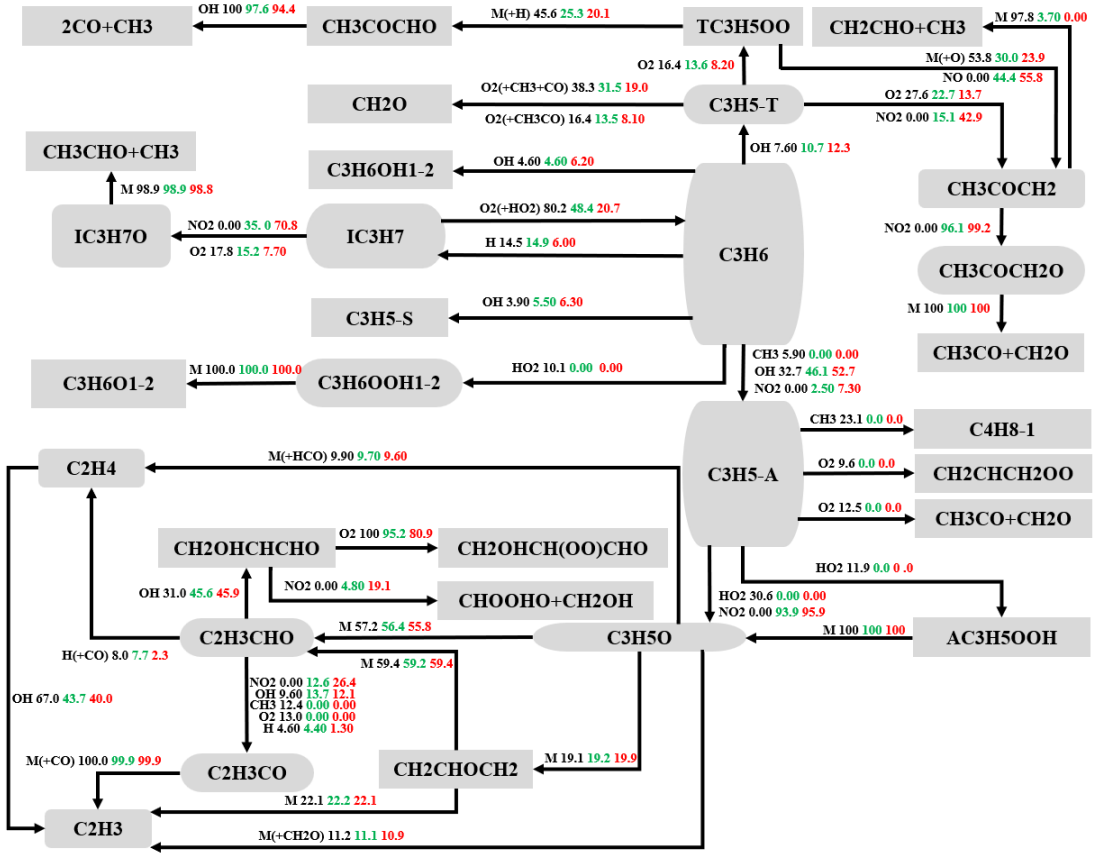

Figure 13 Flux analysis for stoichiometric C_3H_6/NO_2 mixtures at 1.01E+6 Pa, 1000 K and 10% C_3H_6 consumption using the updated model. ($N_{0/1.0}$: Black, $N_{30/1.0}$: Green and $N_{100/1.0}$: Red)

6 Conclusions

This study investigates the NO_2 blending effects on the autoignition characteristics of propylene by characterizing the autoignition behavior of $C_3H_6/O_2/Ar$ mixtures in a shock tube at pressures of 2.03E+5 - 1.01E+6 Pa, temperatures of 950 – 1820 K, equivalence ratios of 0.5 – 2.0, and three NO_2 blending ratios (0, 3000, and 10000 ppm). Experimental results reveal the strong and non-linear promoting effects of NO_2 on propylene system's reactivity, with stronger impact observed at higher pressures, lower temperatures, and fuel-leaner conditions. These effects quickly diminish at fuel-rich and higher temperature conditions.

An improved kinetic model is proposed, incorporating the updated rate parameters for

the direct interactions between NOx and propylene and its primary derivatives. The updated model shows much better performance than the existing chemistry models in capturing the NO_2 blending effects, both quantitatively and qualitatively, at all conditions studied in this work, and replicates commendably the reported fundamental experiments in existing studies.

Further kinetic analyses including sensitivity analysis and flux analysis highlight the importance of NOx interacting chemistry that leads to the diverse NO_2 blending effects. Specifically, there is a clear shift in the consumption of C_3H_6 and its primary derivatives (e.g., C_3H_5-A, C_3H_5-T and IC_3H_7) toward the direct interacting channel $R+NO_2=RO+NO$ when NO_2 is blended, which considerably promotes the system's reactivity. On the other hand, with NO_2 addition, $NO_2 + H = NO + OH$ competes with the chain branching reaction $O_2 + H <=> O + OH$, particularly at high temperatures, which suppresses the system's reactivity.

Acknowledgement

The authors would like to thank the support from the Heilongjiang Provincial Natural Science Foundation (LH2020E067), the National Science and Technology Major Project (2019-III-0014-0058, J2019-III-0012-0055), the Fundamental Research Funds for the Central Universities (3072022TS0309), and the Hong Kong Scholars Award grant number 18.

References

[1] M. Pan, W. Qian, H. Wei, D. Feng, J. Pan, Effects on performance and emissions of gasoline compression ignition engine over a wide range of internal exhaust gas recirculation rates under lean conditions, *Fuel* 265 (2020) 116881.

[2] M. Krishnamoorthi, R. Malayalamurthi, Z. He, S. Kandasamy, A review on low temperature combustion engines: Performance, combustion and emission characteristics, *Renew. Sust. Energ. Rev.* 116 (2019) 109404.

[3] A. Dubreuil, F. Foucher, C. Mounaı, G. Dayma, P. Dagaut, HCCI combustion: Effect of NO in EGR, *Proc. Combust. Inst.* 31 (2007) 2879-2886.

[4] J. Masurier, F. Foucher, G. Dayma, P. Dagaut, Investigation of iso-octane combustion in a homogeneous charge compression ignition engine seeded by ozone, nitric oxide and nitrogen dioxide, *Proc. Combust. Inst.* 35 (2015) 3125-3132.

[5] Z. Zheng, Z. Lv, A new skeletal chemical kinetic model of gasoline surrogate fuel with nitric oxide in HCCI combustion, *Appl. Energ.* 147 (2015) 59-66.

[6] Y. Kawabata, T. Sakonji, T. Amano, The effect of NOx on knock in spark-ignition engines, Report No. 0148-7191, SAE Technical Paper, 1999.

[7] W. Han, C. Yao, Research on high cetane and high octane number fuels and the mechanism for their common oxidation and auto-ignition, *Fuel* 150 (2015) 29-40.

[8] C.L. Rasmussen, A.E. Rasmussen, P. Glarborg, Sensitizing effects of NO_x on CH_4 oxidation at high pressure, *Combust. Flame* 154 (2008) 529-545.

[9] Z. Chen, P. Zhang, Y. Yang, M.J. Brear, X. He, Z. Wang, Impact of nitric oxide (NO) on n-heptane autoignition in a rapid compression machine, *Combust. Flame* 186 (2017) 94-104.

[10] O. Mathieu, J.M. Pemelton, G. Bourque, E.L. Petersen, Shock-induced ignition of methane sensitized by NO_2 and N_2O, *Combust. Flame* 162 (2015) 3053-3070.

[11] R. Sivaramakrishnan, K. Brezinsky, G. Dayma, P. Dagaut, High pressure effects on the mutual sensitization of the oxidation of NO and CH_4–C_2H_6 blends, *Phys. Chem. Chem. Phys.* 9 (2007) 4230-4244.

[12] P. Dagaut, A. Nicolle, Experimental study and detailed kinetic modeling of the effect of exhaust gas on fuel combustion: mutual sensitization of the oxidation of nitric oxide and methane over extended temperature and pressure ranges, *Combust. Flame* 140 (2005) 161-171.

[13] S. Gersen, A. Mokhov, J. Darmeveil, H. Levinsky, P. Glarborg, Ignition-promoting effect of NO_2 on methane, ethane and methane/ethane mixtures in a rapid compression machine, *Proc. Combust. Inst.* 33 (2011) 433-440.

[14] S. Cheng, C. Saggese, S.S. Goldsborough, S.W. Wagnon, W.J. Pitz, Unraveling the role of EGR olefins at advanced combustion conditions in the presence of nitric oxide: Ethylene, propene and isobutene, *Combust. Flame* 245 (2022) 112344.

[15] S. Cheng, C. Saggese, S.S. Goldsborough, S.W. Wagnon, W.J. Pitz, Chemical kinetic interactions of NO with a multi-component gasoline surrogate: Experiments and modeling, *Proc. Combust. Inst.* 39 (2023) 531-540.
[16] A.V. Menon, S. Lee, M.J. Linevsky, T.A. Litzinger, R.J. Santoro, Addition of NO_2 to a laminar premixed ethylene–air flame: Effect on soot formation, *Proc. Combust. Inst.* 31 (2007) 593-601.
[17] J. Giménez-López, M.U. Alzueta, C. Rasmussen, P. Marshall, P. Glarborg, High pressure oxidation of C_2H_4/NO mixtures, *Proc. Combust. Inst.* 33 (2011) 449-457.
[18] F. Deng, Y. Zhang, W. Sun, W. Huang, Q. Zhao, X. Qin, F. Yang, Z. Huang, Towards a kinetic understanding of the NO_x sensitization effect on unsaturation hydrocarbons: A case study of ethylene/nitrogen dioxide mixtures, *Proc. Combust. Inst.* 37 (2019) 719-726.
[19] W. Yuan, L. Ruwe, S. Schwarz, C. Cao, J. Yang, O. Deutschmann, K. Kohse-Höinghaus, F. Qi, Insights into the interaction kinetics between propene and NO_x at moderate temperatures with experimental and modeling methods, *Proc. Combust. Inst.* 38 (2021) 795-803.
[20] F. Deng, F. Yang, P. Zhang, Y. Pan, J. Bugler, H.J. Curran, Y. Zhang, Z. Huang, Towards a kinetic understanding of the NO_x promoting-effect on ignition of coalbed methane: A case study of methane/nitrogen dioxide mixtures, *Fuel* 181 (2016) 188-198.
[21] Y. Zhang, Z. Huang, L. Wei, J. Zhang, C.K. Law, Experimental and modeling study on ignition delays of lean mixtures of methane, hydrogen, oxygen, and argon at elevated pressures, *Combust. Flame* 159 (2012) 918-931.
[22] J. Würmel, E. Silke, H. Curran, M.Ó. Conaire, J. Simmie, The effect of diluent gases on ignition delay times in the shock tube and in the rapid compression machine, *Combust. Flame* 151 (2007) 289-302.
[23] C. Morley, A Chemical Equilibrium Program for Windows (Gaseq), 2020.
[24] R.J. Kee, F.M. Rupley, E. Meeks, J.A. Miller, CHEMKIN-III: A FORTRAN chemical kinetics package for the analysis of gas-phase chemical and plasma kinetics, Sandia National Laboratories, Livermore, CA, USA, 1996.
[25] A.E. Lutz, R.J. Kee, J.A. Miller, SENKIN: A FORTRAN program for predicting homogeneous gas phase chemical kinetics with sensitivity analysis, Sandia National Laboratories, Livermore, CA, USA, 1988.
[26] M. Chaos, F.L. Dryer, Chemical-kinetic modeling of ignition delay: Considerations in interpreting shock tube data, *Int. J. Chem. Kinet.* 42 (2010) 143-150.
[27] A.A.E.-S. Mohamed, S. Panigrahy, A.B. Sahu, G. Bourque, H. Curran, The effect of the addition of nitrogen oxides on the oxidation of ethane: An experimental and modelling study, *Combust. Flame* 241 (2022) 112058.
[28] J. Chai, C.F. Goldsmith, Rate coefficients for fuel+ NO_2: Predictive kinetics for HONO and HNO_2 formation, *Proc. Combust. Inst.* 36 (2017) 617-626.

[29] M.P. Rissanen, S.L. Arppe, R.S. Timonen, Kinetics of several oxygenated carbon-centered free radical reactions with NO_2, *J. Phys. Chem. A* 117 (2013) 3902-3908.

[30] H. Wu, W. Sun, Z. Huang, Y. Zhang, Biphasic sensitization effect of NO_2 on n-C_4H_{10} auto-ignition, *Combust. Flame* 237 (2022) 111844.

[31] P. Dagaut, J. Luche, M. Cathonnet, Experimental and kinetic modeling of the reduction of NO by propene at 1 atm, *Combust. Flame* 121 (2000) 651-661.

[32] M. Hori, N. Matsunaga, N. Marinov, P. William, W. Charles, An experimental and kinetic calculation of the promotion effect of hydrocarbons on the NO-NO_2 conversion in a flow reactor, *Proc. Combust. Inst.* 27 (1998) 389-396.

[33] P. Gokulakrishnan, C.C. Fuller, M.S. Klassen, Experimental and Modeling Study of C_1–C_3 Hydrocarbon Ignition in the Presence of Nitric Oxide, *J. Eng. Gas Turb. Power* 140 (2018) 041509.

[34] D. Davidson, M. Oehlschlaeger, J. Herbon, R. Hanson, Shock tube measurements of iso-octane ignition times and OH concentration time histories, *Proc. Combust. Inst.* 29 (2002) 1295-1301.

[35] J. Zhang, L. Wei, X. Man, X. Jiang, Y. Zhang, E. Hu, Z. Huang, Experimental and modeling study of n-butanol oxidation at high temperature, *Energ. Fuel* 26 (2012) 3368-3380.

[36] S. Dong, K. Zhang, P.K. Senecal, G. Kukkadapu, S.W. Wagnon, S. Barrett, N. Lokachari, S. Panigaphy, W.J. Pitz, H.J. Curran, A comparative reactivity study of 1-alkene fuels from ethylene to 1-heptene, *Proc. Combust. Inst.* 38 (2021) 611-619.

[37] A. Jach, W. Rudy, A. Pękalski, A. Teodorczyk, Assessment of detailed reaction mechanisms for reproduction of ignition delay times of C_2–C_6 alkenes and acetylene, *Combust. Flame* 206 (2019) 37-50.